Machine Learning for Automatic Identification of Pores in Microscopic Images of Weathered Sandstone from Yungang Grottoes

Yuan Cheng [1,2], Jiamei Xue [1,2], Xiuwei Guo [1,2,3], Yue Zhang [1,2], Jizhong Huang [1,2], Haomin Yu [4]

[1] Institute for the Conservation of Cultural Heritage, School of Cultural Heritage and Information Management, Shanghai University, Shanghai, China, 200444 – xjmshu@shu.edu.cn, chengyuan@shu.edu.cn, guoxw@shu.edu.cn, 2019zhangy@shu.edu.cn, hjizhong@shu.edu.cn
[2] Key Laboratory of Silicate Cultural Relics Conservation (Shanghai University), Ministry of Education – xjmshu@shu.edu.cn, chengyuan@shu.edu.cn, guoxw@shu.edu.cn, 2019zhangy@shu.edu.cn, hjizhong@shu.edu.cn
[3] School of Mechanics and Engineering Science, Shanghai University, Shanghai, China, 200444 – guoxw@shu.edu.cn
[4] Department of Computer Science, Aalborg University, Aalborg 9220, Denmark – haominyu@cs.aau.dk

Keywords: Stone Cultural Heritage, Pore Structure, Machine Learning, Backscattered Electron, Image Segmentation.

Abstract

Pores, as one of the channels for water, air, and microorganisms to enter the rock, accelerate the rock weathering process and change the physical and mechanical properties of the rock. Therefore, the study of the microscopic pore structure is of great significance for stone cultural heritage. This paper proposes a multi-scale pore structure characterization method based on backscattered scanning electron microscope (BSE) images, integrating feature engineering and machine learning techniques. First, for each pixel, 16 features are generated to construct a feature engineering. Then, these features are input into four commonly used machine learning models (Random Forest, Support Vector Machine, Multi-Layer Perceptron, Gradient Boosting Decision Tree) to distinguish pore and mineral matrix. To verify the effectiveness of the multi-channel feature input method, we compared the confusion matrix parameters (accuracy, precision, recall, and F1-score) of the four models before and after adding the feature engineering, and found that the indicators of all models increased by 1%-15%. In addition, the study also found that the Random Forest model performed the best. It can effectively segment the pores in different new images, thus could be directly applied to weathered sandstone images, providing data support for the scientific protection of stone cultural heritages.

1. Introduction

As a famous Buddhist sculptural site, the Yungang Grottoes were inscribed on the UNESCO World Heritage List in 2001, reflecting their significant historical, artistic, and cultural value. Yungang Grottoes is mainly composed of sandstone. Due to natural weathering process and anthropogenic influences, invaluable historical information on the surfaces of many grottoes has been lost (Liu et al., 2011). Therefore, it is of great significance to understand the weathering mechanisms of the grottoes, evaluate the degree of grotto weathering, and thus formulate effective conservation and restoration strategies accordingly.

The microscopic pore structure of sandstone plays a crucial role in the weathering process of cultural heritage. These pores provide pathways for water, air, and microorganisms to infiltrate the rock interior, thereby influencing water and heat transfer within the rock matrix (Hao et al., 2022; Zhao et al., 2024). The pore structure also determines the permeability and mechanical properties of sandstone. Furthermore, pore characteristics are established parameters for quantifying the degree of rock weathering (Zhang et al., 2024a). Consequently, analysis of the microscopic pore structure in weathered sandstone is essential for elucidating weathering mechanisms and developing effective conservation and restoration strategies.

Traditional methods for studying the internal pore structure of rocks include nuclear magnetic resonance (NMR), mercury intrusion porosimetry, and physical adsorption methods (Benavente et al., 2021). For example, Xin et al. (2022) studied the pore structure of sandstone through NMR measurements and fractal analysis. However, these methods can only provide bulk measurements for the entire sample and make it difficult to reveal local details. In recent years, imaging techniques such as thin-section microscopic analysis, X-ray computed tomography (CT), and scanning electron microscopy (SEM) have been widely adopted to image porous media such as sandstone (Liu et al., 2024; Ni et al., 2021). Traditional image processing algorithms, such as threshold segmentation, the watershed algorithm, and the K-Means algorithm, can analyze mineral images based on visual information such as color, brightness, and texture (Wei et al., 2023; Zhang et al., 2017). However, when dealing with complex textures and boundaries, the operation processes of these algorithms are complex, which limits the processing efficiency and performance.

Machine learning (ML) methods can significantly improve pore identification efficiency while reducing manual operation complexity. Several studies have applied ML algorithms for pore structure analysis, including random forest-based segmentation for sandstone CT images (Wang & Sun, 2021; Zhang et al., 2024b). Traditional single-feature extraction methods have limitations when dealing with complex pore characteristics of sandstone. To achieve more accurate analysis, this paper adopts a machine-learning-based image segmentation method with multi-channel feature engineering. We apply this approach to four machine learning models and evaluate their performance using confusion matrix parameters for identifying pores in weathered sandstone of the Yungang Grottoes.

2. Data

The Yungang Grottoes, as shown in Figure 1, are located on the south side of Wuzhou Mountain, about 16 km southwest of Datong City, Shanxi Province, China. The sandstone core samples we used in this study are samples of natural weathering

from the Yungang Grottoes. The diameter of the core is about 50mm. The cores are cut and polished along the cross-section direction, and finally made into thin-slice samples and placed in the instrument to obtain images.

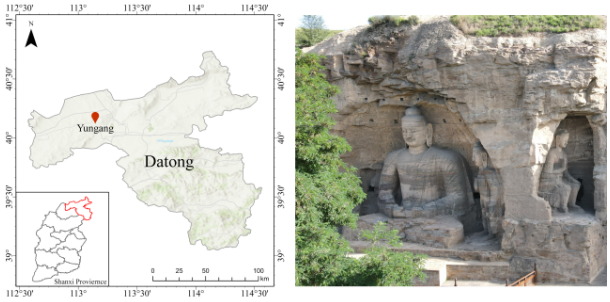

Figure 1. The location of the study area in Datong City, Shanxi Province.

In the backscattered electron imaging (BSE) mode of Scanning Electron Microscopy (SEM), images can be obtained by detecting high-energy electrons scattered from the sample surface in the direction of the electron beam source (Klein et al., 2012). So we finally use BSE images to study the multi-scale porous structure of rock samples.

3. Methodology

The objective of this study is to develop a method for automatically identifying pores based on BSE images. The workflow, as shown in Figure 2, mainly includes pixel-by-pixel annotation and creation of pore labels, multi-channel feature extraction, construction and division of the dataset, training and evaluation of the model, and finally applying the model to the images of weathered sandstone in the Yungang Grottoes to verify its effectiveness.

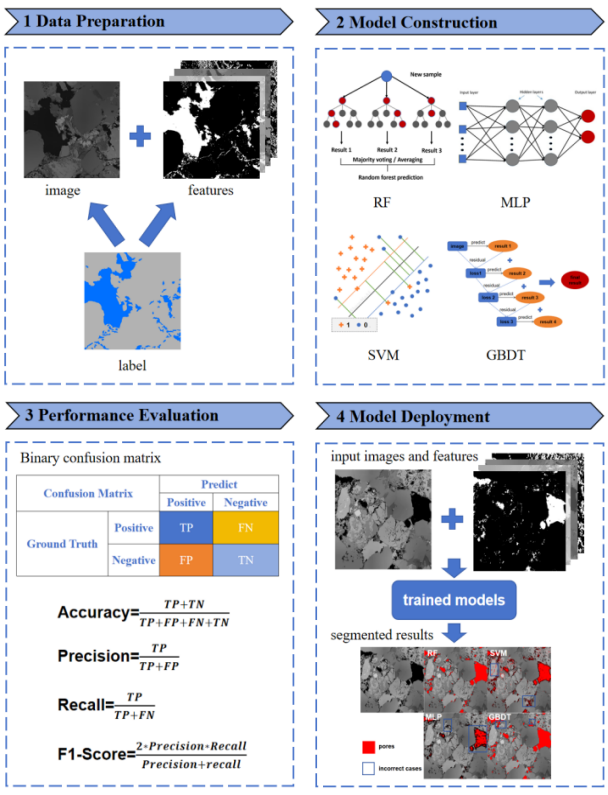

Figure 2. The Workflow of this study.

The performance of machine learning models are influenced by the training dataset. The pixels within the pore components are manually annotated. The machine will define other components in the same image as non-pore components, namely matrix. After selecting the training pixels, multiple features are extracted for each pixel. The data is divided into a training dataset required for training the classifier and a validation dataset for verifying the performance of the classifier at a ratio of 8:2.

3.1 Construction of Feature Engineering

Pixel grayscale can be used as a feature to distinguish different parts in an image. For example, the traditional threshold segmentation method operates based on this feature. However, the pore structure of sandstone is complex. Training a model relying solely on a single feature is likely to result in poor segmentation performance. The pore edge feature can help identify the boundary between pores and non-pores, which is beneficial for outlining the pore regions in the sandstone structure. The grayscale gradient, representing the rate of change of grayscale, can reveal the fine-scale changes within the pore and non-pore regions. In the frequency domain, the spectral distribution of grayscale can visually display the intensities of different frequency components in the image, by means of which pores and non-pores can be distinguished. Analyzing the grayscale relationship between each pixel and its neighboring pixels helps to further identify the texture characteristics of pores. Therefore, increasing the number of features can capture the complex information of the pore structure from different dimensions, which is crucial for improving the performance of the segmentation model and achieving a more accurate analysis of the sandstone pore structure.

In this study, eight types of transformations are used to construct the feature engineering, namely image inversion, logarithmic transformation, contrast enhancement, image binarization, bilateral filtering, Roberts operator, hessian matrix, and wavelet transforms. These features describe each pixel and its adjacent area based on multi-resolution spatial and scale-related information. The classifier uses this information to assign pore labels to each specific pixel in the image.

3.1.1 Image Inversion: As shown in Figure 4(a), image inversion is used to obtain the inverted image of an image with pixel values in the range of [0, L], which is regarded as a feature. This method can enhance the white or grey areas in the image, especially when black dominates the image. The formula for image inversion transformation is as follows:

$$s = L - 1 - r \tag{1}$$

where r = original pixel value
s = transformed pixel value
L − 1 = maximum grayscale of the image pixels

3.1.2 Logarithmic Transformation: Image logarithmic transformation can yield one feature. Its main function is to compress the dynamic range. Logarithmic transformation can expand the low grayscale part of the image, and revealing more details in this part. Meanwhile, it can compress the high grayscale part of the image, and reduce the details in this part. Therefore, logarithmic transformation can enhance the darker part of the image. The formula for logarithmic transformation is:

$$s = c\log(1 + r) \quad (2)$$

where r = original pixel value
s = transformed pixel value
c = principal distance

3.1.3 Contrast Enhancement: Stretching the grayscale to the entire range of 0-255 can significantly enhance the contrast of the image, which is called contrast enhancement. By stretching the grayscale details of the feature objects as needed, the grayscale intervals of interest can be enhanced. There are various methods for contrast enhancement. In this paper, a feature is obtained by using piece - wise linear transformation, and the specific transformation formula is:

$$y = \begin{cases} m_1 \cdot x + b_1 & \text{if } x_1 \le x \le x_2 \\ m_2 \cdot x + b_2 & \text{if } x_3 \le x \le x_4 \end{cases} \quad (3)$$

where m_1 = slope of the first linear segment
b_1 = intercept of the first linear segment
m_2 = slope of the first linear segment
b_2 = intercept of the first linear segment

3.1.4 Image Binarization: Image binarization sets the grayscale of pixels in an image to either 0 or 255, making the entire image appear in distinct black and white colors. By setting a threshold, pixels with grayscale greater than this threshold are set to the maximum grayscale (usually 255), and pixels with grayscale less than this threshold are set to the minimum grayscale (usually 0), thus achieving binarization. Image binarization yields one feature. The traditional threshold segmentation method uses this approach to segment images (Garg & Garg, 2013). Commonly used binarization methods include the bimodal method, the mean method, and Otsu's method, etc. In this paper, Otsu's method is adopted. It is a clustering-based image binarization method that separates the foreground and background pixels of an image by calculating the optimal threshold, maximizing the inter-class variance. Figure 4(b) shows the binarized image.

3.1.5 Bilateral Filtering: Bilateral filtering yields one feature, and it adds a pixel values' weight term based on Gaussian filtering. That is to say, both the distance factor and the influence of pixel values' differences need to be considered. The more similar the pixel values are, the greater the weight. For example, in a window centered on q, the calculation formulas for the pixel weight and the spatial distance weight of a point p during the filtering process are as follows:

$$G_s = \exp\left(-\frac{||p-q||^2}{2\sigma_s{}^2}\right) \quad (4)$$

$$G_r = \exp\left(-\frac{\left|I_p - I_q\right|^2}{2\sigma_r{}^2}\right) \quad (5)$$

The filtering result of the entire filter is:

$$BF = \frac{1}{w_q}\sum_{p\in S} G_s(p)G_r(p) * I_p \quad (6)$$

where w_q= sum of the weights of each pixel value

3.1.6 Roberts Operator: The Roberts operator uses local difference operators to find edges. It approximates the gradient magnitude by the differences between two adjacent pixels in the diagonal direction to determine whether the current point is an edge, thus obtaining edge features. However, it is sensitive to noise. The Roberts operator uses two 2x2 templates: (-1 0, 0 1) and (0 -1, 1 0) to perform convolution operations on the image, and calculate the grayscale differences in the horizontal and vertical directions respectively. By calculating the sum of the absolute values of the gray differences in the two directions, the edge intensity can be obtained.

3.1.7 Hessian Matrix: In image analysis, we can regard an image as a continuous function, where the value of each pixel is the output of the function. The first-level derivative of an image represents the change in image grayscale, namely the grayscale gradient, and the second-level derivative represents the degree of change of the grayscale gradient. In practical applications, the Hessian matrix is calculated by convolving the image with the second-order derivatives of the Gaussian kernel in the x and y directions. Since edges usually correspond to areas where the image grayscale gradient changes significantly, this method can be used to extract the edge features of an image. Based on the neighborhood of the pixel defined by the function $f(x, y)$, three features, namely H_{xx}, H_{xy} and H_{yy} are calculated at each pixel location.

The Hessian matrix applied to a two-dimensional image $f(x, y)$ is expressed as:

$$H[f(x,y)] = \begin{bmatrix} H_{xx} & H_{xy} \\ H_{yx} & H_{yy} \end{bmatrix} \quad (7)$$

where $H_{xx} = \frac{\partial^2 f}{\partial x^2}$, which represents the second order rate of change of the image function $f(x, y)$ in the x-direction.

$H_{xy} = \frac{\partial^2 f}{\partial x\,\partial y} = H_{yx} = \frac{\partial^2 f}{\partial y\,\partial x}$, which represents the result of first taking the partial derivative of the function $f(x, y)$ with respect to x and then taking the partial derivative with respect to y.

$H_{yy} = \frac{\partial^2 f}{\partial y^2}$, which represents the second order rate of change of the image function $f(x, y)$ in the y-direction.

3.1.8 Wavelet Transforms: Wavelet transform conducts multi-resolution spatial scale analysis of signals and can decompose images layer by layer. It uses a series of wavelets of different scales to decompose the original function. The result after transformation is the coefficients of the original function under wavelets of different scales, which can match different spatial frequencies in the image. Medium and low spatial frequencies usually match the image content, while high frequency coefficients usually represent noise or texture regions.

Figure 3 shows a schematic diagram of the two-layer wavelet decomposition of an image. LL_1 and LL_2 represent the low-frequency components. LH_1 and LH_2 represent the high-frequency components in the horizontal direction of the first layer and the second layer respectively. HL_1 and HL_2 represent the high-frequency components in the vertical direction of the first layer and the second layer respectively. HH_1 and HH_2 represent the high-frequency components in the diagonal direction of the first layer and the second layer respectively. The low-frequency part retains the general appearance information of the original image, while the high- frequency component part contains the detailed information of the image.

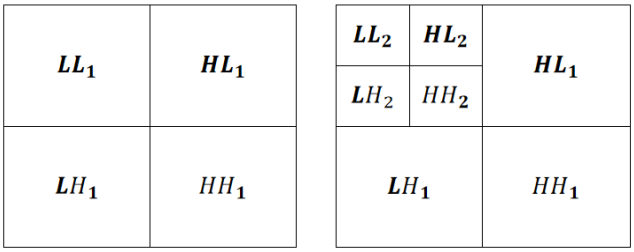

Figure 3. Wavelet transforms generated in the first layer and the second layer.

For image segmentation, we finally obtain the details in the horizontal, vertical, and diagonal directions of the image after two-layer wavelet decomposition. Figure 4(c) and (d) show the high-frequency details in the vertical and horizontal directions of the one-layer wavelet decomposition of the image respectively. We don’t use LL_1 and LL_2 as features of the image because they are merely blurred versions of the original image, which are not suitable for distinguishing pores from matrix components nor for accurately identifying pore contours. For each pixel in the image, we finally generate six features.

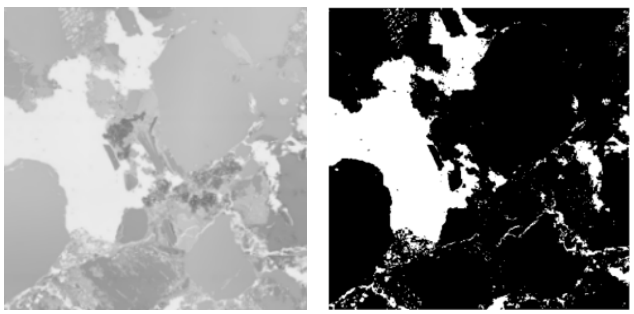

(a) Image inversion (b) Image binarization

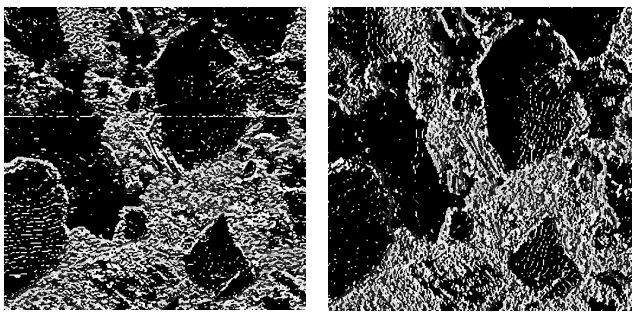

(c) HL_1 (d) LH_1

Figure 4. Examples of features extracted from one SEM image after the first level of processing.

3.2 Machine Learning Models for Image Segmentation

Based on the above 16 features and labels, several commonly used machine learning models were trained to segment the images of weathered sandstone in the Yungang Grottoes, including Random Forest, Support Vector Machine, Multi-Layer Perceptron, and Gradient Boosting Decision Trees.

Random Forest (RF) is an ensemble learning model based on the Bagging strategy. It can effectively handle non-linear problems and over-fitting issues. Moreover, it can effectively deal with a large number of samples and features, enhancing the generalization ability of the model. Random Forest also has a certain degree of interpretability. The prediction results of the model can be explained through feature importance. These characteristics make Random Forest has excellent application effects in many practical problems.

Support Vector Machine (SVM) is a supervised learning algorithm that can be used for classification and regression tasks. In image segmentation, SVM is usually applied to classification. Its core idea is to find the optimal classification hyperplane in the training dataset, so that misclassified samples are as far away from the classification hyperplane as possible. This process can be achieved by maximizing the margin between the support vectors. SVM is often used to handle high dimensional data and performs particularly well when the number of samples is small.

Multi-Layer Perceptron (MLP) is a feed-forward neural network that typically consists of an input layer, one or more hidden layers, and an output layer. During the training process, the pixel feature vectors are fed into the network through the input layer. In the hidden layers, each node applies weights and activation functions to the input data to generate an output. The output of the network is compared with the actual labels to calculate the error. Finally, the back propagation algorithm is used to adjust the weights in the network to reduce the error. The MLP optimizes the weights through multiple iterations until the network can classify pixels with a high degree of accuracy.

Gradient Boosting Decision Trees (GBDT) is an iterative decision tree algorithm. It optimizes an accumulative prediction function iteratively. At each step, a new weak learner is constructed for the residual of the previous round (that is, the difference between the true value and the predicted value). Specifically, in each iteration, the model calculates the negative gradient of the residual as the new learning target, trains a decision tree to fit this gradient, and adds the new tree to the accumulative function with an appropriate learning rate. In this way, Gradient Boosting Decision Trees gradually reduce the residual, and can obtain better prediction performance and generalization ability than a single model while maintaining the simplicity of the model.

3.3 Model Evaluation

The constructed training dataset was put into each model for training , and the validation dataset was put into the model to verify the model's performance. By calculating and comparing the confusion matrix parameters of each model, namely accuracy, precision, recall, and F1-score, before and after the addition of feature engineering, we select the model that is most suitable for the pore segmentation of weathered sandstone images in the Yungang Grottoes for subsequent discussion and research.

The Confusion Matrix is a visualization tool for evaluating machine learning models, mainly used to compare the differences between predicted results and actual results. The structure of the confusion matrix for a binary classification problem is shown in Figure 5. We consider both the predicted value and the true value as 1 or 0. In the confusion matrix, TP (True Positive) refers to the situation where the model predicts 1 and the true value is also 1. TN (True Negative) refers to the situation where the model predicts 0 and the true value is also 0. FP (False Positive) refers to the situation where the model predicts 1, but the true value is 0. FN (False Negative) refers to the situation where the model predicts 0 while the true value is 1.

Confusion Matrix		Predict	
		Positive	Negative
Ground Truth	Positive	TP	FN
	Negative	FP	TN

Figure 5. Binary confusion matrix.

For a large amount of data, from the confusion matrix, we can obtain more advanced classification metrics, namely Accuracy, Precision, Recall, and F1_Score. Among them, Accuracy represents the proportion of correctly identified samples by the model to the total number of samples. Precision is the proportion of samples that are actually positive among all the samples predicted as positive by the model. Recall measures how many of all the true positive samples are correctly identified by the model. F1_Score is defined as the harmonic mean of precision and recall, considering recall and precision to be equally important. Generally, the closer these metrics are to 1, the better the model performance. The calculation formulas for the above-mentioned metrics are as follows:

$$\text{Accuracy} = \frac{TP+TN}{TP+FP+FN+TN} \tag{8}$$

$$\text{Precision} = \frac{TP}{TP+FP} \tag{9}$$

$$\text{Recall} = \frac{TP}{TP+FN} \tag{10}$$

$$\text{F1\_Score} = \frac{2 * \text{Precision} * \text{Recall}}{\text{Precision} + \text{recall}} \tag{11}$$

4. Results and Discussion

4.1 Performance of Different Models

The parameters of the confusion matrix are used to compare the differences between the predicted results and the actual results. As shown in Table 1, the accuracy, precision, recall, and F1-Score of the four models on the training set are presented. Among them, the Random Forest stands out with the best performance across various indicators, boasting an accuracy, precision, recall, and F1 - Score all as high as over 99%.

Model	Accuracy	Precision	Recall	F1_Score
RF	**99.99%**	**99.97%**	**99.99%**	**99.98%**
SVM	97.82%	80.11%	81.84%	80.97%
MLP	98.28%	87.56%	81.08%	84.20%
GBDT	98.28%	89.11%	79.33%	83.93%

Table 1. Quantitative evaluation of the method proposed in this paper on training datasets.

Before and after the addition of feature engineering, the performance of the four models varied. The specific data of various evaluation indicators are detailed in Table 2. It can be seen from the table that after incorporating feature engineering, the performance of all models has improved. The recall and F1-score of all models have increased by 1% - 15% to varying degrees, indicating that the models' ability to identify pores has been enhanced and they can complete the segmentation more accurately and comprehensively. At the same time, the precision of each model has also increased. For example, the precision of SVM has increased from 79.26% to 86.74%, enhancing the reliability of the model in segmenting pores.

Model		RF (%)	SVM (%)	MLP (%)	GBDT (%)
Accuracy	before	97.64	97.48	97.64	97.64
	after	98.33	98.12	98.28	98.28
Precision	before	87.29	79.26	85.90	87.38
	after	90.53	86.74	87.60	89.09
Recall	before	68.27	75.01	69.82	68.35
	after	78.68	78.77	81.22	79.43
F1_Score	before	76.62	77.08	77.03	76.70
	after	84.19	82.56	84.28	83.98

Table 2. Quantitative evaluation of the four models proposed in this paper before and after feature engineering.

4.2 Pores Segmentation Results

In order to evaluate the generalization ability of the proposed models, all of them were applied to segment new images. The segmentation results are shown in Figure 6. The areas within the blue rectangular frames are where the model's segmentation performance is poor. For example, the Support Vector Machine misidentifies the matrix as pores, the Multi-Layer Perceptron fails to fully recognize the pore contours, and the Gradient Boosting Decision Tree connects independent pores during recognition. In conclusion, the Random Forest has the best segmentation effect.

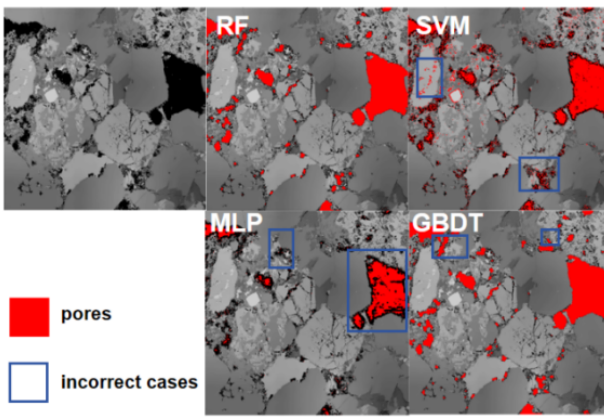

Figure 6. Segmentation results on new images.

To further verify the generalization and stability of the random forest model, it was employed to segment other new images. The segmentation results are shown in Figure 7, with the red regions denoting the pore components. The model has basically achieved the identification of pores. Consequently, it can be directly applied to the BSE images of weathered sandstone samples from the Yungang Grottoes, which in turn facilitates the subsequent extraction of pore parameters of different weathered sandstones.

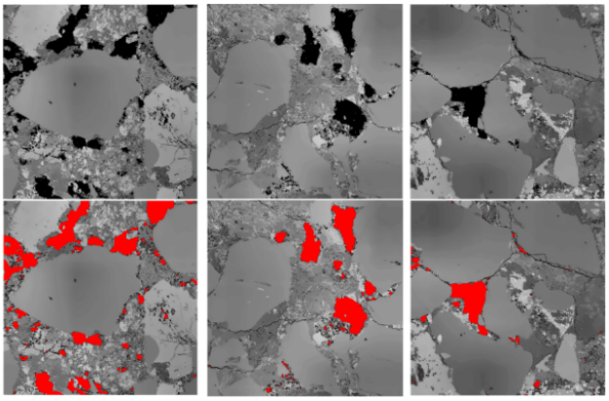

Figure 7. Application of the trained model on other BSE images of sandstone samples.

5. Conclusion

In this study, a machine learning-based feature extraction and model construction method is proposed to efficiently identify the pore components in the backscattered electron (BSE) images of weathered sandstone samples. A multi-channel feature input method is adopted to construct the feature engineering, and the performance of four models (Random Forest, Support Vector Machine, Multi-Layer Perceptron, Gradient Boosting Decision Tree) before and after the addition of feature engineering is evaluated on the training set and the validation set. The study finds that the performance indicators of the models after adding feature engineering have increased by 1% - 15% respectively on the validation set. Among them, the Precision of the Support Vector Machine has increased from 79.26% to 86.74%. Among all these trained models, the Random Forest performs the best, with all indicators in the training set reaching over 99%, and the Precision of the validation set is as high as 98.33%. When apply the four models to segment new images, it is found that the Random Forest has the best segmentation effect, with strong model generalization ability, good applicability and application value. In future research, the established feature engineering will continue to be explored and optimized, and attempts will be made to combine it with deep learning technology to further improve the accuracy and efficiency of pore extraction from weathered sandstone samples of the Yungang Grottoes.

Acknowledgements

This research was supported by Scientific and Technological Research Project of Cultural Relics of State Administration of Cultural Heritage (No. 2023ZCK014), Project of Key Laboratory of Silicate Cultural Relics Conservation (Shanghai University), Ministry of Education (No. SCRC2024KF06YQ, SCRC2024ZZ02ZD), Science and Technology Major Special Program Project of Shanxi Province (No. 202201150501024) and the Tencent Tanyuan Program 2024. The authors thank Yungang Research Institute for providing assistance and support with data acquisition, and Shanghai Technical Service Center of Science and Engineering Computing at Shanghai University for computational resources.

References

Benavente, D., Such-Basañez, I., Fernandez-Cortes, A., Pla, C., Cazorla-Amorós, D., Cañaveras, J. C., & Sanchez-Moral, S. (2021). Comparative analysis of water condensate porosity using mercury intrusion porosimetry and nitrogen and water adsorption techniques in porous building stones. *Construction and Building Materials, 288*, 123131. .

Garg, N., & Garg, N. (2013). Binarization techniques used for grey scale images. *International Journal of Computer Applications, 71*(1), 8-11. .

Hao, J., Qiao, L., Liu, Z., & Li, Q. (2022). Effect of thermal treatment on physical and mechanical properties of sandstone for thermal energy storage: a comprehensive experimental study. *Acta Geotechnica, 17*(9), 3887-3908. 10.1007/s11440-022-01514-8.

Klein, T., Buhr, E., & Georg Frase, C. (2012). Chapter 6 - TSEM: A Review of Scanning Electron Microscopy in Transmission Mode and Its Applications. In P. W. Hawkes (Ed.), *Advances in Imaging and Electron Physics* (Vol. 171, pp. 297-356): Elsevier..

Liu, D., Cao, K., Tang, Y., Zhang, J., Meng, X., Ao, T., & Zhang, H. (2024). Study on weathering corrosion characteristics of red sandstone of ancient buildings under the perspective of non-destructive testing. *Journal of Building Engineering, 85*, 108520. .

Liu, R. Z., Zhang, B. J., Zhang, H., & Shi, M. F. (2011). Deterioration of Yungang Grottoes: Diagnosis and research. *Journal of Cultural Heritage, 12*(4), 494-499. doi.org/10.1016/j.culher.2011.03.008.

Ni, H., Liu, J., Huang, B., Pu, H., Meng, Q., Wang, Y., & Sha, Z. (2021). Quantitative analysis of pore structure and permeability characteristics of sandstone using SEM and CT images. *Journal of Natural Gas Science and Engineering, 88*, 103861. doi.org/10.1016/j.jngse.2021.103861.

Wang, Y., & Sun, S. (2021). Multiscale pore structure characterization based on SEM images. *Fuel, 289*, 119915. doi.org/10.1016/j.fuel.2020.119915.

Wei, X.-D., Deng, Z.-Q., Li, Q., Huang, Y., & Zhao, G.-F. (2023). A 3D grain-based reconstruction method from a 2D surface image for the Distinct Lattice Spring Model. *International Journal for Numerical and Analytical Methods in Geomechanics, 47*(11), 2027-2048. doi.org/10.1002/nag.3549.

Xin, Y., Wang, G., Liu, B., Ai, Y., Cai, D., Yang, S., . . . Chen, K. (2022). Pore structure evaluation in ultra-deep tight sandstones using NMR measurements and fractal analysis. *Journal of Petroleum Science and Engineering, 211*, 110180. doi.org/10.1016/j.petrol.2022.110180.

Zhang, P., Lu, S., Li, J., Zhang, P., Xie, L., Xue, H., & Zhang, J. (2017). Multi-component segmentation of X-ray computed tomography (CT) image using multi-Otsu thresholding algorithm and scanning electron microscopy. *Energy Exploration & Exploitation, 35*(3), 281-294. 10.1177/0144598717690090.

Zhang, R., Huang, J., Cheng, Y., & Zhang, Y. (2024a). Machine learning based prediction for bulk porosity and static elastic modulus of Yungang Grottoes sandstone. *Heritage Science, 12*(1), 359. .

Zhang, Y., Li, Z., & Wu, H. (2024b). Interactive machine learning for segmenting pores of sandstone in computed tomography images. *Gas Science and Engineering, 126*, 205343. doi.org/10.1016/j.jgsce.2024.205343.

Zhao, Y., Qin, W., Jin, A., Wu, H., & Chen, Z. (2024). Research and analysis of the impact of the pore structure on the mechanical properties and fracture mechanism of sandstone. *Materials Today Communications, 38,* 107753. doi.org/10.1016/j.mtcomm.2023.107753.